Modelling of paramagnetic trivalent silicon defect centres in amorphous silica and at Si–SiO_2 interfaces

2005 J. Phys.: Condens. Matter 17 S2099

(http://iopscience.iop.org/0953-8984/17/21/006)

INSTITUTE OF PHYSICS PUBLISHING JOURNAL OF PHYSICS: CONDENSED MATTER

J. Phys.: Condens. Matter **17** (2005) S2099–S2113 doi:10.1088/0953-8984/17/21/006

Modelling of paramagnetic trivalent silicon defect centres in amorphous silica and at Si–SiO_2 interfaces

András Stirling[1] **and Alfredo Pasquarello**[2,3]

[1] Computational Science, Department of Chemistry and Applied Biosciences, ETH Zurich, USI Campus, Via Giuseppe Buffi 13, 6900 Lugano, Switzerland
[2] Ecole Polytechnique Fédérale de Lausanne (EPFL), Institute of Theoretical Physics, CH-1015 Lausanne, Switzerland
[3] Institut Romand de Recherche Numérique en Physique des Matériaux (IRRMA), CH-1015 Lausanne, Switzerland

Received 14 January 2005
Published 13 May 2005
Online at stacks.iop.org/JPhysCM/17/S2099

Abstract

We review the structural and hyperfine properties of Si dangling bond defects occurring in amorphous SiO_2 and at various Si–SiO_2 interfaces. These defects have in common a singly occupied orbital on a trivalent Si centre. We first briefly summarize the most important methodologies for calculating hyperfine parameters, pointing out their advantages and drawbacks. The properties of the defect centres composed of $Si{\equiv}Si_nO_{3-n}$ kernels, with n varying from 0 to 3, are then discussed in a systematic manner. We present three important factors affecting the hybrid state of the unpaired dangling bond: the local geometry around the defect centre, the electronegativity of the first-neighbour atoms, and the polarization effect due to the oxide environment around the dangling bond. We demonstrate that the cage polarization effect significantly increases the Fermi contact term of the defect Si atom, and discuss the relevant implications. We also quantify the interaction between the dangling orbital and the oxygen atoms belonging to the oxide cage by focusing on the ^{17}O hyperfine couplings. For various defects in amorphous SiO_2 and at Si–SiO_2 interfaces, we discuss assignments to $Si{\equiv}Si_nO_{3-n}$ structural units in relation to available experimental data. In particular, we address the charge state of the E'_γ centre, the peculiar hyperfine properties of the S centre, and the atomic structures of the three P_b-type centres.

(Some figures in this article are in colour only in the electronic version)

1. Introduction

A very important class of paramagnetic point defects occurring in Si/SiO_2 based microelectronic devices is those featuring an sp^3 hybrid orbital on a threefold coordinated Si atom. Such defects, which can occur either at the Si–SiO_2 interface or in the oxide,

are responsible for the degradation of the electronic performance of Si-based metal–oxide–semiconductor (MOS) devices. The defect centre is characterized by an $Si{\equiv}Si_nO_{3-n}$ core unit, with n between 0 and 3, which corresponds to the immediate bonding environment of the trivalent Si atom. Numerous experimental techniques have been employed to assess how these defects affect the electrical, optical and transport properties of MOS devices. The most important experimental technique in this field is electron-spin-resonance (ESR) spectroscopy, which offers direct information on the unpaired electron of the defect centre through its g tensor and hyperfine parameters [1, 2]. These properties are interpreted in terms of the interaction of the electron spin with the local environment and with the defect centre. For an accurate interpretation, a detailed understanding of the defect structure and of its electronic properties is therefore indispensable. The information provided by theoretical calculations is crucial in this context. In fact, the identification of most of such defects is generally achieved by matching experimental and theoretical data [2, 3].

The atomic formula identifying the kernel of this family of defects suggests that their properties vary in a systematic manner for n going from 0 to 3. In this work, we mainly focus on the electronic and hyperfine properties. We discuss general mechanisms responsible for the changes in the hybrid state of the dangling bond in the $Si{\equiv}Si_nO_{3-n}$ defect centres, which in turn determine their hyperfine properties. In particular, we focus on the interaction between the dangling bond and its oxide environment. We determine how strongly the oxide cage surrounding the defect affects the dangling bond properties and to what extent the unpaired orbital transfers spin to oxygen atoms of this cage. Then, we discuss in detail the defect properties for n varying from 0 to 3 in relation to the available experimental data. Particular attention is devoted to the $n = 0$ case, which corresponds to the family of E' centres and to the $n = 3$ case, to which the different P_b-type defects belong. In the latter case, we also compare various model structures in relation to the hyperfine characteristics and show that an $Si{\equiv}Si_3$ core constitutes the kernel of all the P_b-type centres. In the case of the P_{b1} centre, we specifically study the effect of various oxide structures on the hyperfine properties and address the ^{17}O superhyperfine (SHF) values.

2. Computational methodologies

Theoretical investigations of the $Si{\equiv}Si_nO_{3-n}$ centres either use cluster [4–36] or periodic model structures [34, 37–46]. Both modelling approaches offer advantages and disadvantages. With periodic models a proper description of the electronic structure in the solid phase can be achieved. In addition, the different types of strains occurring in the network structure are realistically accounted for. However, the simulation cell size in actual calculations renders the theoretical point-defect concentrations often excessively high with respect to the ones in the real systems, and this might lead to undesirable interactions between the defect site and its images. Although the cell size artefact cannot be eliminated, it can be analysed by the consideration of larger simulation cells. A further attractive characteristic of periodic models is that non-zero temperature effects can be simulated and free energy information on formation or transformation mechanisms obtained [42, 45, 46].

Cluster models in point defect studies also have their advantages. The description of the electronic structure is achieved with localized orbitals which are particularly favourable for localized defects. Cluster approaches allow one to use models of moderate size with the possibility of systematically checking the convergence of the calculated properties against the system size. The effect of electron correlation on the calculated properties can also very efficiently be studied on cluster models. Drawbacks of using clusters for modelling point defects are that they cannot represent long-range solid state properties, that the

equivalence of unperturbed atoms of the crystal is not preserved, and that the strain fields are not properly accounted for. These issues are strongly related to the termination of the cluster models. In cluster studies of $Si{\equiv}Si_nO_{3-n}$ defects, the usual approach is to saturate the unsaturated bonds with hydrogen atoms, the positions of which are either kept fixed to mimic the original crystalline environment [5, 19–22] or optimized allowing for full relaxation [9, 34, 70]. For $Si{\equiv}Si_nO_{3-n}$ centres, it has been shown that the cluster size and its termination can significantly affect the calculated hyperfine parameters of the defect [34]. Moreover, cluster models should explicitly include the oxide environment around the defect, the effect of cage polarization being otherwise neglected [34]. An important cluster approach which aims at capturing the relevant structural aspects of the amorphous environment around the trivalent Si defect is the embedded-cluster method [32, 35, 36], in which the core of the system is treated quantum mechanically while the larger, outer part is treated classically.

The periodic models are usually described with electronic structure methods based on density functional theory (DFT) [47]. In order to reduce the computational cost, periodic calculations usually employ pseudopotentials (PPs): either normconserving [48] or ultrasoft ones [49, 50], reducing in this way the number of electrons which are explicitly treated in the calculations. Plane-wave basis sets are generally used in connection with PPs. The energy cutoff, which determines the size of the basis set, strongly depends on the type of adopted pseudopotentials. Non-zero temperature effects can be included by performing *ab initio* molecular dynamics simulations [51]. Activation energies [45] and reaction mechanisms [42] can be studied by using the Blue Moon sampling method [52]. The recently developed metadynamics method [53, 54], which is particularly effective in simulating chemical reactions [55, 56], has recently also been applied to identify specific defect formation pathways [46].

Semiempirical [4, 6–8, 10, 11, 13–16, 31], Hartree–Fock (HF) [9, 12, 17–21, 23, 25–27, 29, 32, 34, 36], post-HF [19, 20] as well as DFT-based methods [5, 21–24, 29, 30, 33–35] have been employed in connection with cluster models in the study of $Si{\equiv}Si_nO_{3-n}$ centres. Structural optimizations and ground state properties have mostly been achieved with semiempirical, HF or DFT methods. Optical properties require more sophisticated methods, and have been accessed with multireference single and double excitations configuration-interaction calculations (MRDCI) [57] or with time-dependent density functional response theory (TD-DFT) [58].

Since ESR spectroscopy provides the most detailed information on the defect structure, the principal contact between theory and experiment is generally the hyperfine spectrum. We briefly review its theoretical computation here. The Hamiltonian describing the ESR spectrum for $Si{\equiv}Si_nO_{3-n}$ defects can be written as

$$H = \mu_B \mathbf{B}\cdot\mathbf{g}\cdot\mathbf{S} + \mathbf{I}\cdot\mathbf{A}\cdot\mathbf{S}, \tag{1}$$

where the first term is the electronic Zeeman interaction, and the second term is the spin–nucleus hyperfine interaction; μ_B is the Bohr magneton, $\mathbf{B}$ the applied external magnetic field, $\mathbf{g}$ the electronic g dyadic, and $\mathbf{A}$ the hyperfine tensor describing the coupling between electronic ($S = 1/2$) and nuclear ($I = 1/2$ for ^{29}Si) spins. The hyperfine parameters of $\mathbf{A}$ can be obtained from the calculated spin densities of the optimized model structures. The elements of $\mathbf{A}$ can be written as $A_{ij} = a\,\delta_{ij} + b_{ij}$, where

$$a = \frac{8\pi}{3} g_e \mu_e g_{Si} \mu_{Si} \rho_s(\mathbf{R}), \tag{2}$$

$$b_{ij} = g_e \mu_e g_{Si} \mu_{Si} \int \rho_s(\mathbf{r}) \frac{3r_i r_j - \delta_{ij}}{r^5}\, d^3\mathbf{r}. \tag{3}$$

Table 1. Representative selection of theoretical ^{29}Si isotropic hyperfine parameters (in gauss) obtained with different methodologies for $Si{\equiv}Si_nO_{3-n}$ centres in various systems.

	$Si{\equiv}O_3$		$Si{\equiv}SiO_2$		$Si{\equiv}Si_3$		
Method and model	E_1'	E_γ'	S	$Si{\equiv}Si_2O$	P_b	P_{b0}	P_{b1}
Cluster							
MINDO/3 [6, 7]	417				142		
HF/DZP [70], $Si(OSiH_3)_x[Si(SiH_3)_3]_{3-x}$		409	252	180	130		
DFT(GGA)/6–311 + G* [34], $Si(OSiH_3)_x(SiH_3)_{3-x}$		389	207	129	78		
HF/6–31G, embedded [35], QM cluster: $Si_{11}O_{33}$	457						
Periodic							
DFT(LDA)/PP/PW [39]	467	515					
DFT(GGA)/PP/PW [34, 41]		501	315	171	130	127	155
DFT(GGA)/PAW/PP [40]	414						
Experimental [72–75, 92]	412	419	279		113	100	127

a is the isotropic (also called Fermi) contact interaction term, while the values b_{ij} arise from the anisotropic dipolar contributions. Here, $\rho_s = \rho_\uparrow - \rho_\downarrow$ is the electron spin density, g_e the electron g factor, μ_e the Bohr magneton, g_{Si} the nuclear gyromagnetic ratio for Si, μ_{Si} the corresponding nuclear magneton, and $\mathbf{r}$ the electron coordination vector with respect to the nuclear site $\mathbf{R}$. Diagonalization of the matrix A_{ij} yields the eigenvalues and the corresponding principal directions.

The calculation of $\mathbf{A}$ requires the electron spin density $\rho_s(\mathbf{r})$ in the core region. While this function is directly available in all-electron calculations, the spin density in the PP schemes has to be recovered at the end of the calculations. Schemes in which the wavefunctions are reconstructed have successfully been applied to both normconserving [59] and ultrasoft [34, 41] PPs. Indeed, it is possible to derive an expression for the reconstructed wavefunctions in terms of the atomic all-electron orbitals and the optimized pseudo wavefunctions [59, 60]. For instance, in the ultrasoft PP scheme, the reconstructed spin density reads:

$$\rho^s(\mathbf{r}) = \sum_i \left[|\phi_i^s(\mathbf{r})|^2 + \sum_{nm,I} Q_{nm}^I(\mathbf{r}) \langle \phi_i^s | \beta_n^I \rangle \langle \beta_m^I | \phi_i^s \rangle \right] \tag{4}$$

where s labels the spin state, the ϕ_i^s are the one-electron spin-dependent pseudo wavefunctions, and the β_n^I and $Q_{nm}^I(\mathbf{r})$ are projector and augmentation functions, respectively. In equation (4), the first term in the brackets describes the *soft* part of the electron density while the second term corresponds to the *hard* contribution which is strictly localized in the core region [50]. The pseudized $Q_{nm}^I(\mathbf{r})$ augmentation functions used in the PP calculations are replaced with their original counterparts. Note that the core states are treated implicitly. Hence core-polarization effects can generally not be accounted for in these reconstruction schemes. Nonetheless, very recent developments provide a general scheme for including these effects in PP calculations [61].

Table 1 offers a comparison between various calculations of the Fermi contact term for the family of trivalent Si centres under investigation in this work. We note a large variation in the calculated values for a given model system. The electronic structure method, the choice of model structure, and the employed basis sets all contribute to the observed spread. The HF-based methods are known to overestimate the hyperfine term by concentrating the electron

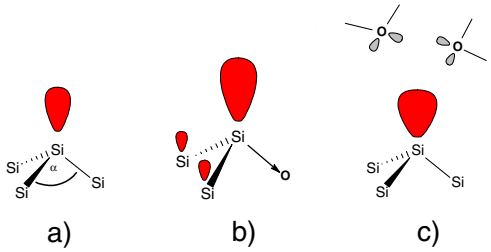

Figure 1. Schematic representation of the principal electronic mechanisms affecting the contact interaction a_{HF} in $Si{\equiv}Si_nO_{3-n}$ defect centres. (a) Local geometry: the sharper the $Si{\equiv}Si_3$ unit, the larger a_{HF}, because of the larger p character of the dangling bond. (b) Electronegativity of neighbouring atoms: (i) a neighbouring atom of large electronegativity in the backbonds increases the p contribution of the defect atom to the backbond, thereby increasing the s character of the dangling-bond orbital and consequently a_{HF}; (ii) spin delocalization, due to an enhanced overlap between the Si–Si backbonds and the dangling bond orbital. (c) Oxide environment: a_{HF} increases because of the Pauli repulsion between the dangling bond and the lone pairs of oxygen atoms in the neighbouring oxide.

density toward the nuclei. The Gaussian-type basis functions cannot satisfy the cusp behaviour of the wavefunctions at the nucleus sites, leading to an underestimation of the isotropic term. In the cluster calculations, excessive relaxation leads to a decrease of the spin density at the nucleus site. Moreover, the electronegativity of the chosen termination may significantly affect the electron distribution. In pseudopotential calculations, the neglect of core-polarization effects leads to overestimations of the Fermi contact term. These considerations emphasize the necessity of careful validating the theoretical results before addressing experimental data [34].

3. General considerations

Before discussing in detail the various defect structures, it is important to review the basic factors which affect the electronic properties of the defect centres, and, consequently, their hyperfine properties. The underlying mechanisms are general and independent of the specific defect composition. We here consider both ^{29}Si and ^{17}O hyperfine interactions.

In this section, we carried out DFT-based calculations on small cluster models in order to identify trends and to estimate orders of magnitude. We used the Perdew–Wang generalized gradient approximation (GGA) for the exchange correlation functional [62] as available in the Gaussian98 program package [63]. The calculations were performed with the 6–311 + G* basis set.

3.1. ^{29}Si hyperfine interactions

The ^{29}Si hyperfine interaction is essentially determined by the ratio of the s and p contributions of the atomic orbitals of the defect Si atom to the unpaired dangling-bond wavefunction. In particular, the isotropic term is solely determined by the degree of s character, because the orbitals of higher angular momenta have a node at the nucleus site, and therefore do not contribute to the spin density at the nucleus. Three important factors contributing to a deviation from the ideal sp^3 hybrid state can be identified: (a) the geometry around the defect atom; (b) the electronegativity of the atoms with which the undercoordinated Si atom forms covalent bonds; and (c) the interaction of the dangling bond with the lone pairs of nearby oxygen atoms belonging to the surrounding oxide network (figure 1).

(a) *Local geometry.* It is well known that the structure around the radical centre has a large influence on the hybrid state of the unpaired orbital. When the bond angles around the trivalent Si atom increase, i.e. the structure assumes a more planar arrangement, the hybrid state of the bonding orbitals becomes more sp^2-like, and consequently the dangling orbital carries more p character. The hyperfine isotropic term of the defect Si atom therefore decreases. In contrast, when the radical centre assumes a 'sharper' structure, the isotropic term becomes larger due to the larger s component in the dangling orbital.

(b) *Electronegativity of neighbouring atoms.* When the defect Si atom forms bonds with other atoms of high electronegativity, two important effects can be observed. First, the isotropic hyperfine term increases. Indeed, when we compare the Fermi contact terms for E'-type centres with those of the various P_b centres, we notice an increase by roughly a factor of three (table 1). In fact, the high electronegativity of the neighbouring atoms increases the p character with which the Si centre participates in the bonding orbital [64]. Consequently, its s contribution decreases in the bonding orbital and increases in the dangling bond, thereby leading to an increase of the Fermi contact term. Second, the high electronegativity of the neighbouring atom provokes a significant spin delocalization over the Si atoms in the first neighbour shell of the defect atom [34, 65]. Due to the increased degree of s character in the dangling bond, the energy level of this bond deepens and its overlap with the Si–Si backbonds is enhanced. This overlap gives rise to the formation of extended orbitals which involve both the defect Si atom and its neighbouring Si atoms. In this way, spin density also appears on the saturated Si atom, rendering it active in ESR measurements. We note that the mechanism responsible for the relatively large spin transfer from the unsaturated to the saturated Si atom is quite general. In fact, we found that atoms of high electronegativity (e.g. F, N, O, Cl) in the first neighbour shell of the defect centre provoke such spin delocalization not only in Si centres but also in the analogous Ge centres [65].

(c) *Oxide environment.* The oxide environment around the trivalent Si atom has a profound effect on the hybrid state of its dangling bond, and thus on the hyperfine properties. In order to estimate the influence of the oxide environment on an $Si{\equiv}Si_nO_{3-n}$ centre, we studied the Fermi contact term as a function of the position of a nearby bonded oxygen atom in the cases of $n = 0$ and 3. The defect centre was modelled by an $Si(SiH_3)_n(OSiH_3)_{3-n}$ cluster. The bonded oxygen atom of the oxide was represented by an H_2O molecule. The dipole moment of the water molecule was oriented radially with respect to the defect atom, with the hydrogen atoms pointing outwards. The results are shown pictorially in figure 2.

We find that a nearby oxygen atom, depending on its distance and its orientation with respect to the dangling bond, causes a 6–29% increase of the isotropic term for an $Si{\equiv}Si_3$ unit, and a 3–16% enhancement for an $Si{\equiv}O_3$ unit. The increase can generally be understood as being due to a Fermi repulsion between the dangling bond and the lone pairs of the oxygen atom. By decreasing the p character of the dangling bond, the defect centre can effectively decrease this repulsion. In this way, the s/p ratio increases in the unpaired hybrid orbital, thereby increasing the spin density at the Si nucleus. The repulsion clearly depends on the distance and on the polar angle relative to the dangling bond direction. The azimuthal displacement has a negligible influence on the Fermi contact term, reflecting the axial symmetry of the unpaired orbital. The enhancement of the Fermi contact term due to the presence of a nearby O atom is more pronounced for the $Si{\equiv}Si_3$ centre than for the $Si{\equiv}O_3$ one. This is due to the fact that the s character in the unpaired orbital of the $Si{\equiv}O_3$ centre is much higher, as shown by the value of the hyperfine terms. Hence, in this case, the dangling bond is more compact and the Pauli repulsion smaller. We also considered the simultaneous presence of a larger number of oxygen

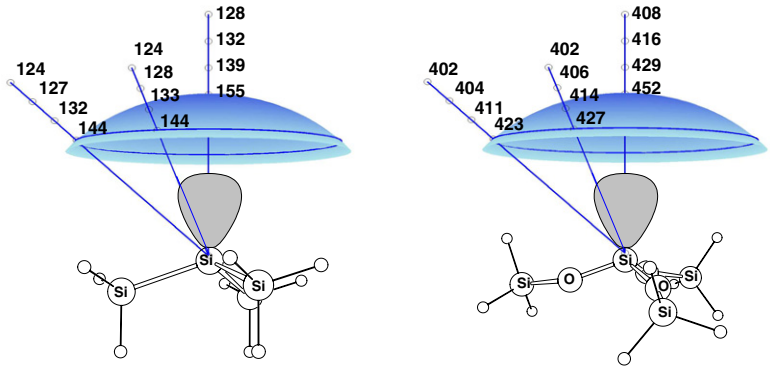

Figure 2. Graphical representation of the effect of the Pauli repulsion between the Si dangling bond and a nearby oxygen atom. The indicated values correspond to calculated Fermi contact terms of the defect Si atom and are shown for oxygen atoms located along three different lines. One line lies along the direction of the dangling bond, another one in the plane formed by the dangling bond and an Si–Si(O) backbond, and the third one in the plane bisecting two Si–Si(O) backbonds. The latter two lines form a polar angle of 45° with respect to the direction of the dangling bond. The surface sphere indicates a distance of 3 Å from the radical centre. The contact terms were calculated at distances of 3.0, 3.5, 4.0 and 4.5 Å from the defect centre. In the absence of nearby oxygen atoms, we calculated hyperfine terms of 117 G for the $Si{\equiv}Si_3$ and of 389 G for the $Si{\equiv}O_3$ model.

atoms. We calculated the isotropic contact terms for the defect atom when surrounded by three oxygen atoms placed at a distance of 3 Å, in the same positions considered above one by one (figure 2). We obtained 174 G for the $Si{\equiv}Si_3$ unit and 468 G for the $Si{\equiv}O_3$ one. Hence, two additional oxygen atoms give an increase of 12% for the $Si{\equiv}Si_3$ unit, but an increase of only 4% for the $Si{\equiv}O_3$ unit. This effect should again be attributed to the different s character of the dangling bond in the two cases. Assuming distances between network oxygen atoms and the defect Si atom falling in the range of 3.5–4 Å, the present results indicate that the effect of the oxide cage surrounding the unpaired orbital may be significant. We therefore conclude that the nearby oxygen atoms should be taken into consideration in a quantitative analysis of ^{29}Si hyperfine interactions. The neglect of this effect leads to an underestimation of the spin density on the defect Si atom. In brief, we conclude that the hybridization state of the dangling bond depends strongly on its immediate bonding as well as on its longer-range, non-bonding environment.

3.2. ^{17}O superhyperfine interactions

The interaction between the dangling-bond state and the oxide environment can also be revealed by focusing on ^{17}O SHF interactions. ESR ^{17}O measurements have indeed been performed to obtain insight into the structure of the oxide environment in the vicinity of the Si dangling orbital [66–69]. In SiO_2 [68] and at $Si(100)$–SiO_2 interfaces [69], no signal could be detected. However, at $Si(111)$–SiO_2 interfaces, the ^{17}O hyperfine investigations gave measurable signals, which were interpreted as arising from the interaction of the dangling bond with either one [66] or two oxygen atoms [67] of the oxide network facing the microvoid around the dangling bond. Using semiempirical calculations, Ong *et al* attempted to provide an interpretation of these experimental data, but a conclusive assignment of the local oxide structure around the dangling bond proved difficult [16].

In order to estimate the extent of the spin transfer from the Si dangling bond to an O atom in the nearby oxide network, we used the same cluster models used above (figure 2) and

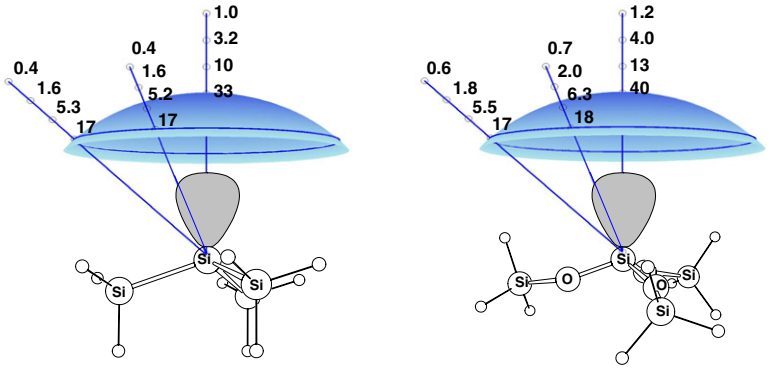

Figure 3. Graphical representation of the dependence of the ^{17}O hyperfine Fermi term (in gauss) of a nearby oxygen atom on its position relative to the dangling bond of an Si≡Si$_3$ and an Si≡O$_3$ centre. The arrangements are the same as in figure 2.

modelled the nearby O atom with an H_2O molecule. The calculated ^{17}O hyperfine interaction is given in figure 3 for various positions of the H_2O molecule. The Fermi contact term on the oxygen nucleus depends strongly on the position of the oxygen atom relative to the defect Si atom. When the oxygen atom does not lie on the axis of the dangling bond, the interaction is weaker and the Fermi term decays very rapidly with distance.

Interestingly, the Si≡O$_3$ centre yields slightly larger SHF values than the Si≡Si$_3$ unit. This is due to the fact that the dangling orbital of the Si≡O$_3$ centre has a lower energy level, owing to the higher s contribution from the defect Si atom. The lower orbital energy favours the interaction with the oxygen orbitals, which occurs at much lower energy. Hence, more spin density appears on the oxygen atoms in this case.

For an Si≡O$_3$ centre in an amorphous oxide environment, the SHF interactions with oxygen atoms belonging to the oxide network need to be compared with the hyperfine interactions associated to oxygen atoms in the backbond of the defect. For our models, we calculated hyperfine interactions of 27–32 G depending on the position of the oxide O atom. Since the closest network oxygen atoms are expected to give SHF values up to 40 G, these results suggest that SHF and hyperfine interactions due to ^{17}O are indistinguishable in amorphous SiO_2.

4. The paramagnetic Si≡Si$_n$O$_{3-n}$ centres

In this section, we discuss various Si≡Si$_n$O$_{3-n}$ centres in relation to available experimental data. In order to present a comprehensive interpretation of the experimentally measured signals, it is imperative to rely on a coherent theoretical scheme, for which the deviations with respect to experiment are well understood.

The DFT calculations discussed in this section were all performed with the PW91 functional [62]. The electronic wavefunctions were expanded on a basis of plane waves. We employed ultrasoft PPs [49, 50] to account for the interaction between the ionic cores and the valence electrons. We considered periodic model structures which were designed with the intent of providing a realistic description of the environment of the defect centre. The atomic positions in all our model structures were fully relaxed by damped molecular dynamics [50, 51]. A detailed description of the adopted model structures is given in [34] and [41].

The ^{29}Si hyperfine interactions calculated within this electronic-structure scheme have been validated through an extensive comparison with all-electron schemes in [34]. This

comparison revealed that the neglect of core-polarization effects in the present scheme leads to overestimations of the contact interaction as large as 10% for the $Si{\equiv}Si_3$ defects, the error being considerably smaller for the other defects of the series. When this effect is accounted for, the results obtained with the present scheme overestimate the experimental data by about 20%. The residual error should be attributed to the approximate exchange–correlation energy and to the neglect of relativistic effects. In the following, our interpretation is based on the assumption that this residual error is systematic, affecting the hyperfine contact interactions of the various core units in the same proportion.

4.1. $Si{\equiv}O_3$: E'-type defects

The defects which are characterized by a dangling bond at an $Si{\equiv}O_3$ unit correspond to the most abundant natural defects in SiO_2 and belong to the family of E'-type centres. They are generally modelled as oxygen vacancy centres, often carrying positive charge. The E'_1 variant in crystalline SiO_2 is described by the generally accepted Feigl–Fowler–Yip model [76, 77]. The unpaired orbital is localized on a threefold coordinated Si atom facing the O vacancy. The other Si atom facing the vacancy bonds to a distant oxygen atom giving rise to a puckered structure with a positively charged threefold coordinated O centre ($O^+{\equiv}Si_3$). A large number of theoretical studies have provided support for this model [7, 8, 12, 13, 15, 32, 35–40, 44, 45].

On the basis of its hyperfine properties [68, 73], the E'_γ defect, a variant of the E'_1 defect occurring in amorphous SiO_2, has been assigned to a similar structural configuration. The E'_γ model also gained considerable theoretical support [4, 17, 19, 23–27, 34, 39]. However, it has recently been pointed out that a different structural configuration, but still featuring a central $Si{\equiv}O_3$ unit, could also account for the ESR characteristics of the E'_γ centre [29, 30, 71].

Unlike the E'_1 centre, several experiments provided evidence that the formation of E'_γ centres does not necessarily require hole trapping, indicating that these defects could be neutral [78–85]. In order to gain insight in how the charge state affects the hyperfine properties of the E'_γ centre, we performed a series of calculations using realistic models of this defect in amorphous SiO_2 [34]. We first considered puckered models in which the $Si{\equiv}O_3$ units are accompanied by a positively charged O atom. We found an average hyperfine Fermi term of 501 G, which compares well with the experimental value of 419 G when the expected overestimation by 20% is taken into account. Then, we considered a model structure in which the puckered Si atom is saturated by a hydride anion, bearing in this way a defect in the neutral charge state. The calculations yielded a Fermi term of 495 G, rather close to the results for the charged models. This agreement clearly indicates that, provided the $Si{\equiv}O_3$ unit is preserved, the charge state of the puckered Si unit does not influence the E'_γ hyperfine properties in a significant way.

4.2. $Si{\equiv}SiO_2$: the S defect

The $Si{\equiv}SiO_2$ centre can be modelled as an oxygen divacancy in SiO_2. The *S* centre, observed in oxygen-deficient amorphous SiO_2 [86, 87], shows a hyperfine spectrum with two detectable doublets at 162 and 279 G, and has tentatively been assigned to the $Si{\equiv}SiO_2$ structural unit [88–92].

Karna and collaborators performed calculations on small cluster models of the $Si{\equiv}SiO_2$ centre, yielding values for the Fermi contact term between 247 and 252 G [25, 26, 70] (table 1). However, these calculations could not explain the presence of a second weak doublet in the experimental spectra. In a recent work [34], calculations on periodic model structures provided an explanation for the observation of two doublets in the hyperfine spectrum of the *S* centre.

The principal doublet arises from the defect Si atom, while the weaker accompanying doublet results from the delocalized spin density on the saturated Si atom in the first-neighbour shell of the defect Si atom. The mechanism at the origin of this spin delocalization effect was briefly discussed in section 3.1. In particular, the calculations yielded isotropic hyperfine interactions of 315 and 202 G, which agree with the experimental values of 279 and 162 G in view of the expected overestimation.

4.3. $Si{\equiv}Si_2O$

So far, the $Si{\equiv}Si_2O$ structural unit has not been assigned unequivocally to any measured defect. In a first interpretation, Stesmans suggested that the lower doublet of the *S* centre might arise from the joint presence of the $Si{\equiv}SiO_2$ and $Si{\equiv}Si_2O$, but the convincing assignment of both doublets to the *S* centre undermines this possibility (cf section 4.2). The $Si{\equiv}Si_2O$ structural unit was also proposed as the central unit of the P_{b1} defect occurring at Si(100)–SiO_2 interfaces [1, 75]. However, this assignment could subsequently be discarded both experimentally and theoretically. We defer a more detailed discussion on this point to the next section.

Since a single oxygen atom is found in the first-neighbour shell of the defect Si atom (cf section 3.1), the experimental isotropic hyperfine interaction should fall between those measured for the $Si{\equiv}SiO_2$ ($\sim$279 G) and $Si{\equiv}Si_3$ units (100–127 G). HF calculations on small clusters situated the contact term for the $Si{\equiv}Si_2O$ defect centre at 180 G (table 1). The present electronic-structure scheme applied to clusters of similar size yielded a lower value of 162 G [34]. In view of the overestimation inherent to the latter approach, the former estimate clearly suffers from excessive spin localization, typical of HF calculations. However, neither estimate accounts for the enhancement due to nearby oxygen atoms of the oxide network (figure 2).

Oxygen atoms belonging to the oxide environment of the hypothetical $Si{\equiv}Si_2O$ defect structure are expected to enhance the isotropic hyperfine interaction with respect to that calculated for small cluster models in table 1. For instance, when an $Si{\equiv}Si_2O$ unit is considered at the Si(100)–SiO_2 interface as for the bridge model in the next section, we found an isotropic hyperfine interaction of 171 G. Instead, a calculation for a small isolated cluster only gives 162 G [34]. The difference of about $\sim$10 G should be attributed to the presence of surrounding oxygen atoms in the oxide (section 3.1).

We also note that an O atom in the first neighbour shell of the defect Si atom induces spin delocalization over the other two first-neighbour Si atoms (section 3.1). We calculated SHF isotropic terms of 16 G on the saturated neighbour Si atoms [34]. This feature might provide an experimental signature for identifying the $Si{\equiv}Si_2O$ defect centre.

4.4. $Si{\equiv}Si_3$: the P_b-type defects at Si–SiO_2 interfaces

$Si{\equiv}Si_3$-type dangling bond centres occur at Si–SiO_2 interfaces as a consequence of the lattice mismatch between the silicon substrate and the oxide overlayer. Depending on the orientation of the Si substrate, ESR measurements identified three different paramagnetic defects: P_b, P_{b0}, and P_{b1}.

The P_b centre occurring at the Si(111)–SiO_2 interface is very well characterized both experimentally [74, 93, 94] and theoretically [5, 6, 10, 22, 41]. The centre is conclusively identified as an sp^3 hybrid on a [111]-oriented interfacial $Si{\equiv}Si_3$ unit.

The P_{b0} defect occurs at the Si(100)–SiO_2 interface. ESR measurements [75, 94–96] revealed that this centre is also composed of an $Si{\equiv}Si_3$ unit on a (111) microfacet, thus featuring

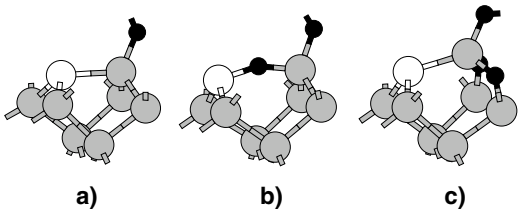

Figure 4. Various atomic structures proposed for the P_{b1} defect centre: (a) strained dimer model; (b) oxygen bridge model; (c) asymmetrically oxidized dimer (AOD) model. Grey balls indicate saturated Si atoms, black balls O atoms, and white balls defect Si atoms.

Table 2. Calculated hyperfine contact terms a_{HF} (in gauss) and angle θ between the dangling bond orientation (as deduced from the hyperfine tensor) and the surface normal for the P_b-type model structures. The hyperfine parameters in parentheses are experimental values from [75].

Defect	Model	a_{HF}	θ
P_b		130 (113)	[111] ([111])
P_{b0}		127 (100)	[111] ($\langle 111\rangle$)
P_{b1}	Dimer	126 (127)	21° (32.3°)
	Bridge	171 (127)	30° (32.3°)
	AOD	155 (127)	33° (32.3°)

a physico-chemical structure identical to that of the P_b defect. This assignment gained support from a theoretical study in which such a defect structure was incorporated in a realistic model of the Si(100)–SiO_2 interface [41]. The value of 127 G calculated for the isotropic hyperfine interaction shows good agreement with the experimental result of 100 G [75] (cf table 2).

The Si(100)–SiO_2 interface also shows another defect involving an Si dangling bond, known as the P_{b1} centre. A complete experimental characterization of the P_{b1} defect has been achieved only very recently. Early experimental observations pointed to a defect structure very similar to that of the P_{b0} centre. However, accurate hyperfine measurements revealed that the axis of the Si dangling bond forms an angle of 32° with the interface normal [75]. Since this orientation does not correspond to any bonding direction of the silicon crystal, this observation suggests that the interface structure is significantly reconstructed at the P_{b1} location. Experimentally, Brower carried out ^{17}O hyperfine measurements which did not reveal any significant signature due to oxygen atoms in the immediate neighbourhood of the defect Si atom [69]. From the theoretical point of view, Edwards proposed an $Si{\equiv}Si_3$-type structure with a strained Si–Si bond for this defect, on the basis of semiempirical and HF calculations on small clusters [9].

The detailed experimental characterization of the P_{b1} defect [75] motivated the reconsideration of its atomic structure in a recent theoretical study [41]. The hyperfine parameters were calculated for various defect structures located within realistic models of the Si(100)–SiO_2 interface [97–99]. Previous suggestions in the literature [9, 100] led to the consideration of the strained dimer model (figure 4). For this model, a contact term of 126 G was calculated, in apparent good agreement with the measured value of 127 G [75]. However, in view of the expected systematic overestimation of the calculated result by about 20%, this result in reality reveals excessive p character in the dangling bond orbital. This is understood on the basis that the strained environment of the $Si{\equiv}Si_3$ unit favours a more planar configuration, leading to a more sp^2-like bonded structure (cf section 3.1). The inadequacy of the dimer model is further supported by the orientation of the dangling bond with respect

Table 3. Hyperfine contact term a_{HF} (in gauss) and dangling bond orientation θ calculated for various AOD model structures.

Oxide	a_{HF}	θ
Tridymite	155	33°
β-crystobalite	152	37°
No oxide	116	34°

to the normal: the calculation gives an angle of 21°, significantly lower than the experimental angle of 32° [75] (cf table 2).

Along the lines of an early proposal [94], an oxygen bridge model was then taken under consideration in order to examine the effect of an oxygen atom in the first coordination shell of the defect Si atom (figure 4). This model structure yields an isotropic hyperfine interaction of 171 G, larger than the experimental value of 127 G [75] by 34%. Despite the good agreement for the orientation of the dangling bond (table 2), the size of this deviation is too large to be accounted for by systematic errors inherent to the adopted PP calculation. Hence, this result supports a P_{b1} centre based on an Si≡Si_3 unit [41].

The search for an alternative atomic structure featuring the Si≡Si_3 core unit finally led to the proposal of a novel model for the P_{b1} centre [41]: the asymmetrically oxidized dimer (AOD) (figure 4). This structure yields hyperfine parameters in very good agreement with experiment (table 2). In fact, the overestimation of the contact interaction found for the AOD structure (22%) is fully consistent with a similar overestimation (15%) found for the P_b centre at the Si(111)–SiO_2 interface [41]. Furthermore, the direction of the hyperfine axis of the dangling bond in the AOD model ($\theta = 33°$) agrees closely with the experimental orientation ($\theta = 32°$) [75].

In the AOD model, the correct orientation of the dangling bond is achieved without requiring O atoms in the first-neighbour shell of the defect Si atom, in accord with ^{17}O hyperfine measurements by Brower [69]. However, in comparison with the strained dimer model (figure 4), the two oxygen atoms in the backbonds have an important role in bringing the theoretical hyperfine parameters in closer agreement with the experimental ones. First, those oxygen atoms tilt the Si–Si dimer, increasing the angle θ between the axis of the dangling bond and the surface normal. Second, their presence releases the strain in the Si≡Si_3 core, thereby allowing the dangling bond to carry an enhanced s contribution.

The hybrid state of the dangling bond in an Si≡Si_3 unit carries the largest p contribution among the Si≡Si_nO_{3-n} defects, as every Si-O bond contributes to increasing of the s character of the dangling bond (cf section 3.1). Consequently, the Si≡Si_3 centre is the most sensitive to the effect resulting from the polarization of the oxide network (cf figure 1). We investigated the role of the oxide by analysing how the nature of the oxide affects the hyperfine contact term in the case of the P_{b1} centre. We considered three models, all featuring the AOD core unit but showing different oxide structures. In addition to the original model based on a tridymite structure for the oxide [97, 99, 98], we considered another model with a β-crystobalite oxide structure [98, 101] and a third one in which the oxide is completely removed. In the latter case, the free terminations of the surface and of the AOD core were saturated with H atoms. The calculated hyperfine contact terms for these three models are given in table 3. Upon variation of the oxide environment, we observe that the structure of the defect core unit is only slightly affected, as manifested by the small variations (at most 4°) in the dangling bond orientation. However, the hyperfine contact term a_{HF} shows a remarkable behaviour. The value of a_{HF} is weakly dependent on the oxide structure, showing variations of only 2 G, but decreases by 25% when the oxide is removed. This effect should be attributed to oxygen atoms of the oxide

network which significantly alter the hybrid state of the dangling bond. Our results suggest that it is the mere presence of the oxide that affects the value of a_{HF} rather than the detailed location of the oxygen atoms. The variation by 35–40 G observed upon the removal of the oxide is fully consistent with the results obtained in section 3.1.

For the oxygen atoms in the backbonds of the AOD model, we calculated isotropic ^{17}O SHF values of less than 1.5 G. On the other hand, the oxygen atoms of the oxide network in the close vicinity of the defect atom feature ^{17}O SHF values ranging between 2 and 10 G. Hence, the presence of the backbond oxygen atoms cannot be disputed on the basis of Brower's ^{17}O hyperfine measurements [69], since their SHF interactions are indistinguishable from those of other oxygen atoms of the oxide (cf section 3.2).

5. Concluding remarks

The theoretical properties of the $\mathrm{Si}{\equiv}\mathrm{Si}_n\mathrm{O}_{3-n}$ centres have been reviewed. The systematic variation of their hyperfine properties for n varying between 0 and 3 have been explained by invoking three electronic mechanisms: the effect of the local geometry around the defect centre, the electronegativity of the first neighbour atoms, and the polarization effect of the oxide environment around the dangling bond. We found that the oxide environment has a significant impact on the unpaired dangling orbital, affecting the ^{29}Si hyperfine contact term in detectable manner. Furthermore, we addressed a series of issues associated to specific assignments, such as the charge state of the E'_γ centre, the hyperfine characteristics of the S centre, and the atomic structure of the P_{b1} centre. In particular, we provide evidence in favour of assigning the atomic structures of all P_b-type centres to an $\mathrm{Si}{\equiv}\mathrm{Si}_3$ core unit.

References

[1] Poindexter E H and Caplan P J 1983 *Prog. Surf. Sci.* **14** 201
[2] Weeks R A 1994 *J. Non-Cryst. Solids* **179** 1
[3] Edwards A H and Fowler W B 1999 *Microelectron. Reliab.* **39** 3
[4] O'Reilly E and Robertson J 1983 *Phys. Rev.* B **27** 3780
[5] Cook M and White C T 1987 *Phys. Rev. Lett.* **59** 1741
Cook M and White C T 1988 *Phys. Rev.* B **38** 9674
[6] Edwards A H 1987 *Phys. Rev.* B **36** 9638
[7] Rudra J K and Fowler W B 1987 *Phys. Rev.* B **35** 8223
[8] Edwards A H, Fowler W B and Feigl F J 1988 *Phys. Rev.* B **37** 9000
[9] Edwards A H 1988 *The Physics and Chemistry of SiO_2 and the SiO_2 Interface* ed C R Helms and B E Deal (New York: Plenum) p 271
[10] Edwards A H 1989 *Appl. Surf. Sci.* **39** 309
[11] Chu A X and Fowler W B 1990 *Phys. Rev.* B **41** 5061
[12] Sim F, Catlow C R A, Dupuis M and Watts J D 1991 *J. Chem. Phys.* **95** 4215
[13] Chu A X and Fowler W B 1991 *Phys. Rev.* B **43** 9199
[14] Dianov E M, Sokolov V O and Sulimov V B 1992 *J. Non-Cryst. Solids* **149** 5
[15] Snyder K C and Fowler W B 1993 *Phys. Rev.* B **48** 13238
[16] Ong C K, Harker A H and Stoneham A M 1993 *Interface Sci.* **1** 139
[17] Edwards A H, Fowler W B and Elicker T S 1997 *Mater. Sci. Forum* **239–241** 11
[18] Pacchioni G, Ferrari A M and Ieranò G 1997 *Faraday Discuss.* **106** 155
[19] Pacchioni G, Ieranò G and Márquez A M 1998 *Phys. Rev. Lett.* **81** 377
[20] Pacchioni G, Ieranò G and Márquez A M 1998 *Phys. Rev.* B **57** 818
[21] Pacchioni G and Vitiello M 1998 *Phys. Rev.* B **58** 7745
[22] Tuttle B 1999 *Phys. Rev.* B **60** 2631
[23] Pacchioni G and Vitiello M 1999 *J. Non-Cryst. Solids* **245** 175
[24] Courtot-Descharles A, Paillet P and Leray J L 1999 *J. Non-Cryst. Solids* **245** 154
[25] Karna S P and Kurtz H A 1999 *Microelectron. Eng.* **48** 109

[26] Karna S P, Kurtz H A, Shedd W M, Pugh R D and Singaraju B K 1999 *IEEE Trans. Nucl. Sci.* **46** 1544
[27] Pineda A C and Karna S P 2000 *J. Phys. Chem.* A **104** 4699
[28] Pacchioni G 2000 *Solid State Sci.* **2** 161
[29] Uchino T, Takahashi M and Yoko T 2000 *Phys. Rev.* B **62** 2983
[30] Uchino T, Takahashi M and Yoko T 2001 *Phys. Rev. Lett.* **86** 5522
[31] Grisenko V A, Novikov Yu N, Shaposhnikov A V and Morokov Yu N 2001 *Semiconductors* **35** 1041
[32] Edwards A H, Sushko P V, Shluger A L and Sulimov V B 2002 *IEEE Trans. Nucl. Sci.* **49** 1383
[33] Raghavachari K, Ricci D and Pacchioni G 2002 *J. Chem. Phys.* **116** 825
[34] Stirling A and Pasquarello A 2002 *Phys. Rev.* B **66** 245201
[35] Mysovsky A S, Sushko P V, Mukhopadhyay S, Edwards A H and Shluger A L 2004 *Phys. Rev.* B **69** 085202
[36] Mukhopadhyay S, Sushko P V, Stoneham A M and Shluger A L 2004 *Phys. Rev.* B **70** 195203
[37] Allan D C and Teter M P 1990 *J. Am. Ceram. Soc.* **73** 3247
[38] Carbonaro C M, Fiorentini V and Massica S 1997 *J. Non-Cryst. Solids* **221** 89
[39] Boero M, Pasquarello A, Sarnthein J and Car R 1997 *Phys. Rev. Lett.* **78** 887
[40] Blöchl P 2000 *Phys. Rev.* B **62** 6158
[41] Stirling A, Pasquarello A, Charlier J-C and Car R 2000 *Phys. Rev. Lett.* **85** 2773
Stirling A, Pasquarello A, Charlier J-C and Car R 2000 *Physics and Chemistry of SiO_2 and the Si–SiO_2 Interface-4* ed H Z Massoud, I J R Baumvol, M Hirose and E H Poindexter (Toronto: The Electrochemical Society) p 283
[42] Donadio D, Bernasconi M and Boero M 2001 *Phys. Rev. Lett.* **87** 195504
[43] Lu Z-Y, Nicklaw C J, Fleetwood D M, Schrimpf R D and Pantelides S T 2002 *Phys. Rev. Lett.* **89** 285505
[44] Pickard C J and Mauri F 2002 *Phys. Rev. Lett.* **88** 086403
[45] Boero M, Oshiyama A and Silvestrelli P L 2003 *Phys. Rev. Lett.* **91** 206401
[46] Donadio D and Bernasconi M 2005 *Phys. Rev.* B **71** 073307
[47] Kohn W and Sham L J 1965 *Phys. Rev.* **140** A1133
[48] Pickett W E 1989 *Comput. Phys. Rep.* **9** 115
[49] Vanderbilt D 1990 *Phys. Rev.* B **41** 7892
[50] Pasquarello A, Laasonen K, Car R, Lee C and Vanderbilt D 1992 *Phys. Rev. Lett.* **69** 1982
Laasonen K, Pasquarello A, Car R, Lee C and Vanderbilt D 1993 *Phys. Rev.* B **47** 10142
[51] Car R and Parrinello M 1985 *Phys. Rev. Lett.* **55** 2471
[52] Carter E A, Cicotti G, Hynes J T and Kapral R 1989 *Chem. Phys. Lett.* **156** 472
[53] Laio A and Parrinello M 2002 *Proc. Natl Acad. Sci. USA* **99** 12562
[54] Iannuzzi M, Laio A and Parrinello M 2003 *Phys. Rev. Lett.* **90** 238302
[55] Stirling A, Iannuzzi M, Laio A and Parrinello M 2004 *Chem. Phys. Chem.* **5** 1558
[56] Stirling A, Iannuzzi M, Parrinello M, Molnar F, Bernhart V and Luinstra G A 2004 submitted
[57] Buenker R J and Peyerimhoff S D 1974 *Theor. Chim. Acta* **35** 33
Buenker R J, Peyerimhoff S D and Butscher W 1978 *Mol. Phys.* **35** 771
[58] Runge E and Gross E K U 1984 *Phys. Rev. Lett.* **52** 997
[59] Van de Walle C G and Blöchl P E 1993 *Phys. Rev.* B **47** 4244
[60] Boero M, Oshiyama A and Silvestrelli P L 2004 *Mod. Phys. Lett.* **18** 707
[61] Yazyev O V, Tavernelli I, Helm L and Röthlisberger U 2005 *Phys. Rev.* B at press
[62] Perdew J P, Chevary J A, Vosko S H, Jackson K A, Pederson M R, Singh D J and Fiolhais C 1992 *Phys. Rev.* B **46** 6671
[63] Frisch M J *et al* 1998 *Gaussian 98, Revision A.11.1* (Pittsburgh, PA: Gaussian)
[64] Bent H A 1961 *Chem. Rev.* **61** 275
[65] Stirling A and Pasquarello A 2004 in preparation
[66] Stathis J H 1991 *Solid State Commun.* **79** 119
[67] Stesmans A and Vanheusden K 1991 *Phys. Rev.* B **44** 11353
[68] Griscom D L 1980 *Phys. Rev.* B **20** 4192
[69] Brower K L 1987 *Z. Phys. Chem. (Leipzig)* **151** 177
[70] Karna S P, Kurtz H A, Pineda A C, Shedd W M and Pugh R D 2000 *Defects in SiO_2 and Related Dielectrics: Science and Technology* ed G Pacchioni, D L Griscom and L Skuja (New York: Kluwer–Academic)
[71] Uchino T 2001 *Curr. Opin. Solid State Mater. Sci.* **5** 517
[72] Jani M G, Bossoli R B and Halliburton L E 1983 *Phys. Rev.* B **27** 2285
[73] Griscom D L 1979 *Phys. Rev.* B **20** 1823
[74] Brower K 1983 *Appl. Phys. Lett.* **43** 1111
[75] Stesmans A, Nouwen B and Afanas'ev V V 1998 *Phys. Rev.* B **58** 15801
[76] Feigl F J, Fowler W B and Yip K L 1974 *Solid State Commun.* **14** 225

[77] Rudra J K and Fowler W B 1987 *Phys. Rev.* B **35** 8223
[78] Conley J F Jr, Lenahan P M, Ewans H L, Lowry R K and Morthorst T J 1884 *J. Appl. Phys.* **76** 2872
[79] Afanas'ev V V and Stesmans A 2000 *J. Phys.: Condens. Matter* **12** 2285
[80] Warren W L, Lenahan P M, Robinson B and Stathis J H 1988 *Appl. Phys. Lett.* **53** 482
[81] Afanas'ev V V, de Nijs J M M, Balk P and Stesmans A 1995 *J. Appl. Phys.* **78** 6481
[82] Zvanut M E, Feigl F J, Fowler W B, Rudra J K, Caplan P J, Poindexter E H and Zook J D 1989 *Appl. Phys. Lett.* **54** 2118
[83] Herve D, Leray J-L and Devine R A B 1992 *J. Appl. Phys.* **72** 3634
[84] Mrstik B J, Afanas'ev V V, Stesmans A, McMarr P J and Lawrence R K 1999 *J. Appl. Phys.* **85** 6577
[85] Afanas'ev V V, Stesmans A, Revesz A G and Hughes H L 1998 *J. Electrochem. Soc.* **145** 3157
[86] Holzenkämpfer E, Richter P W, Stuke J and Voget-Grote U 1979 *J. Non-Cryst. Solids* **32** 327
[87] Griscom D L, Friebele E J, Long J K and Fleming J W 1983 *J. Appl. Phys.* **54** 3743
[88] Stesmans A and Afanas'ev V V 1996 *Appl. Phys. Lett.* **69** 2056
[89] Stesmans A and Afanas'ev V V 1997 *Microelectron. Eng.* **36** 201
[90] Stesmans A, Nouwen B and Afanas'ev V V 2002 *Phys. Rev.* B **66** 045307
[91] Stesmans A, Nouwen B, Pierreux D and Afanas'ev V V 2002 *Appl. Phys. Lett.* **80** 4753
[92] Stesmans A, Pierreux D and Afanas'ev V V 2003 *Radiat. Eff. Defects Solids* **158** 419
[93] Nishi Y 1971 *Japan. J. Appl. Phys.* **10** 52
[94] Caplan P, Poindexter E, Deal B and Razouk R 1979 *J. Appl. Phys.* **50** 5847
[95] Rong F C, Harvey J F, Poindexter E H and Gerardi G J 1993 *Appl. Phys. Lett.* **63** 920
[96] von Bardeleben H J, Schoisswohl M and Cantin J L 1996 *Colloids Surf.* A **115** 277
[97] Pasquarello A, Hybertsen M and Car R 1995 *Phys. Rev. Lett.* **64** 1024
[98] Pasquarello A, Hybertsen M and Car R 1996 *Phys. Rev.* B **53** 10942
[99] Pasquarello A, Hybertsen M and Car R 1996 *Appl. Phys. Lett.* **68** 625
[100] Stesmans A and Afanas'ev V V 1999 *Microelectron. Eng.* **48** 113
[101] Pasquarello A, Hybertsen M and Car R 1996 *Appl. Surf. Sci.* **104** 317